Focus Sweep for the New COS/FUV Cenwave G140L/800

Ravi Sankrit[1], William J. Fischer[1], Camellia R. Magness[1], and Andrew J. Fox[1]

[1] Space Telescope Science Institute, Baltimore, MD

8 July 2019

ABSTRACT

The focus setting for the new central wavelength mode G140L/800/FUVA was determined based on a focus sweep program executed in 2018 March. The target AV 75, an O5.5 supergiant star in the Small Magellanic Cloud, was observed at a number of focus settings. The resulting spectra were analyzed to characterize the variation of astigmatic height and the widths of absorption lines as functions of the focus position. The condition for the optimal focus setting was to obtain a balance between minimizing the astigmatic height of the spectral image at the short-wavelength end while retaining adequate spectral resolution at all wavelengths. It was determined that, based on these criteria, the optimal focus value for the mode is -1487 absolute focus steps. In this ISR we describe the focus sweep program (PID 15451) and the data analysis, and we present the results.

Contents

1. Introduction

The central wavelength setting G140L/800 was one of two new modes offered for the COS far-ultraviolet (FUV) channel in Cycle 26. It places the wavelength range from 800 to 1950 Å on detector segment A, and observations are obtained with segment B turned off. More importantly, it places wavelengths shortward of ≈1100 Å on a region of the detector where the extent of the two-dimensional (2D) spectrum of a point source in the cross-dispersion direction due to astigmatism (i.e., the astigmatic height) is small. The smaller astigmatic height significantly reduces the background, which, for faint sources, allows a higher S/N to be reached in the 912–1100 Å wavelength region than with the previously available G140L/1280 mode. The sharp drop in reflectivity of the HST MgF_2/Al primary mirror at ≈1150 Å implies that the short-wavelength regions have inherently low count rates relative to the rest of the spectral range. Enabling the observation of faint sources at these short wavelengths is the primary scientific motivation for cenwave 800.

The mode was first explored in an outsourced calibration program (PID 12501, PI S. McCandliss), with observations obtained while COS was still operating at lifetime position 1 (LP1). A preliminary characterization of the mode is presented in Redwine et al. (2016). Since COS is now operating at LP4, a complete suite of calibration programs were implemented in order to commission the new mode.

The first calibration program was a focus sweep to obtain the focus position for cenwave 800, which was required for all subsequent observations using the mode. While the basic design of the program and the observations are similar to earlier focus sweep programs (e.g., Lennon et al. 2010; Ghavamian 2012; Oliveira et al. 2013; Fox et al. 2015, 2017), the criteria for deciding the optimal focus position for the cenwave 800 mode are different from all previous cases. For other modes, the focus position is chosen to maximize the spectral resolution. In contrast, for cenwave 800, the primary goal is to minimize the height of the spectrum in the cross-dispersion direction at short wavelengths, with the secondary condition of limiting the degradation of the spectral resolution. Therefore, the effects of moving the focus on the spectral shape in both the cross-dispersion and the dispersion directions require analysis.

The unique characteristics of cenwave 800 spectra that we describe here were important in determining the design of programs and the data analyses undertaken for commissioning the mode. In addition to describing the focus sweep, this document also serves as a reference for the Instrument Science Reports on the other cenwave 800 calibration programs.

2. Program Design and Implementation

The focus sweep program consists of a series of spectra obtained at several focus offset positions, measured as steps of the Optics Select Mechanism 1 (OSM 1). The absolute focus position that maximizes the spectral resolution depends on both the grating and the cenwave setting. Previous focus sweep programs have been guided by the results of ray-trace models in determining the likely best focus. However, there were no ray-trace models calculated for the cenwave 800 mode until after the design and execution of the program. Instead, the focus positions at LP4 for G140L/1105, -413 absolute steps (Fox et al. 2017), and for G140L/1280, offset by $+389$ steps relative to cenwave 1105 (Table 7 of Fox et al. 2015) were linearly extrapolated, and the initial estimate of the focus offset for cenwave 800 was determined to be -1087 absolute steps (Figure 1). This zero-point is the focus position at which the spectral resolution is expected to be maximized, and the program was designed to sample this and several values on either side of it.
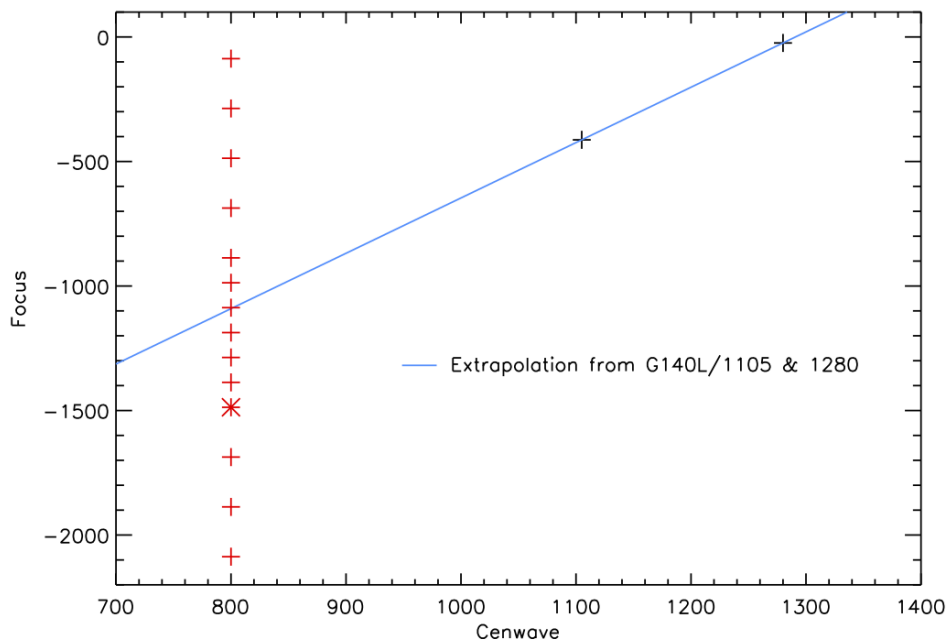

Figure 1. Extrapolation of the focus setting from other G140L modes. The red crosses are the commanded focus offsets in the observing program, and the the the star (-1487) is the focus position chosen for the cenwave 800 mode. Note that we would not expect the cenwave 800 focus to follow the line since the criteria to determine the best focus are different from those used for the other cenwaves.

Spectra obtained for the G140L/1105 focus sweep program (PID 14874) were analyzed to characterize the trends in the cross-dispersion profile widths on detector segment A with changes in the focus offset. This was done to help guide the selection of

focus values at which the cenwave 800 focus sweep was performed. Figure 2 is a plot of the profile widths against the focus offset at three wavelength locations. The G140L/800 and G140L/1105 modes both use only detector segment A, and a given position on the detector along the dispersion direction corresponds to wavelengths separated by about 305 Å for these two modes. The curves for 1200 and 1400 Å in the figure are the closest in wavelength to the region of interest (912–1100 Å) in the cenwave 800 mode. At 1200 Å the cross-dispersion width starts increasing with positive changes in focus offset starting at approximately −300 relative to the zero-point. This suggested the need for a bias towards negative offsets in the program design.
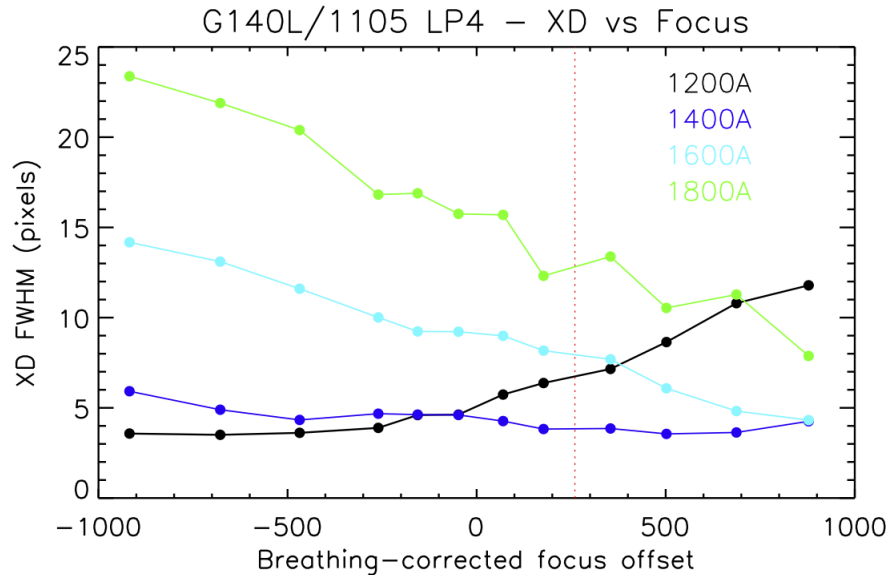

Figure 2. Profile widths in the cross-dispersion direction of G140L/1105/FUVA focus sweep spectra (Program ID 14874), used to guide the cenwave 800 focus sweep design. The red dotted line is the best-fit focus for cenwave 1105 found by Fox et al. (2017).

The observing strategy was to check focus steps ranging from −1000 to +1000 relative to the zero-point of −1087 absolute focus steps. The typical spacing for focus sweeps is to use increments of 200 steps at the extremes, and 100 steps around the zero-point, which is the expected location for the best focus. For the cenwave 800 program, the finer sampling was used between focus offsets of −400 and +200. The thermal breathing of the telescope may introduce differences of up to 100 steps between the actual focus and the commanded focus, so further granularity is unwarranted. The focus offsets specified in our observing program are shown in Figure 1. Anticipating our results, the star symbol indicates the focus position chosen for the cenwave 800 mode.

Our target was AV 75, an O5.5 supergiant star in the Small Magellanic Cloud, which has been used for previous G140L/1105 focus sweep programs (Fox et al. 2017). Since the target is in a crowded field, with several nearby bright field objects, the observing sequence started with an ACQ/SEARCH with specific ORIENT

constraints. An initialization exposure set up the instrument mode to G140L/1105, the nearest available to G140L/800. Then, the focus was moved to an absolute focus position of -2087 (equivalent to -1000 steps from the extrapolated zero-point for c800) and the OSM1 rotation position was set explicitly to the offset between the cenwave 800 and cenwave 1105 positions (OSMROT1=17), and a spectrum was obtained. These steps were repeated, sweeping over the focus values specified. Further details about the telescope and instrument commands required when using a new mode are given in the Phase II proposal for the program (PID 15451, PI W. Fischer).

To determine the exposure time required for the observations, we required that the counts per pixel (dispersion direction) in the low-wavelength region matched those obtained in the cenwave 800 LP1 calibration program (12501). In that program, the target star AV 243 was observed for 1056 s at each focus position. FUSE spectra of the two stars show that AV 243 is about 60% as bright as AV 75 over the 900–1100 Å range. However, the sensitivity of the grating had declined by about 20% since the time of the earlier observations (De Rosa et al. 2018). To obtain the same number of counts requires $1056 \times 0.6 \times 1.2 = 760$ s. In our program, filling the orbits to increase the S/N resulted in 940 s exposures at each focus position.

3. Observations and Data Reduction

The focus sweep observations of AV 75 were successfully executed on 2018 March 23, on a single visit with five orbits. All the observations were obtained at FP-POS=3, the nominal position used to define the central wavelength associated with a mode. The file rootnames, start times (UT), and the commanded focus positions for each exposure are listed in Table 1. (Note that the absolute focus position is equal to the offset position *minus* 1087.) Also listed are the focus positions corrected for the thermal breathing of the telescope. It is these corrected values that we use in the analyses, and they will be discussed in more detail in Section 4.

The data were calibrated by running the pipeline, CalCOS (v3.3.4), on the raw data files (`*rawtag_a.fits`) to obtain corrected events lists files (`*corrtag_a.fits`), which were used for the analysis. The headers of the rawtag files were updated to change the CENWAVE keyword to 1105 (a valid entry is required for CalCOS to run), and FLATFILE to `gw_impostor_flat.fits`, the gridwire flat-field reference file derived for LP4. Since only the `corrtag` files were required for the analysis and the mode had not yet been commissioned, several major steps (heliocentric Doppler correction, 1D spectral extraction, background subtraction, wavelength zero-point adjustment, and flux calibration) were omitted.

The 2D images were created from the `corrtag` files, which contain a list of events and their associated properties, including their weights (EPSILON) that account for the flat-field and deadtime corrections. First, the events were screened to include only those with pulse heights in the 2–23 range by masking out those with data quality flag DQ=512. Then, a 16384×1024 image array was defined in (XCORR, YCORR),

Table 1. Focus Sweep Program for G140L/800: Exposure Log and Focus Offsets

File (ROOTNAME)	Start Time (UT) 2018-03-23	Commanded Focus Offset[1]	Breathing-Corrected Focus Offset[1]
lds101wtq	13:39:23	−1000	−938.4
lds101wvq	13:59:01	−800	−740.6
lds101wyq	14:49:05	−600	−606.3
lds101x0q	15:08:45	−400	−377.1
lds101x2q	15:28:21	−300	−248.3
lds101x4q	16:24:29	−200	−198.9
lds101x6q	16:44:05	−100	−43.7
lds101x8q	17:03:43	0	+66.7
lds101xaq	17:59:51	+100	+109.8
lds101xcq	18:19:27	+200	+259.0
lds101xeq	18:39:07	+400	+465.1
lds101xgq	19:35:11	+600	+612.7
lds101xiq	19:54:51	+800	+856.1
lds101xkq	20:14:29	+1000	+1064.8

[1]Subtract 1087 from these values to convert to absolute focus steps.

the detector co-ordinates corrected for thermal and geometric distortions. (This step requires cropping out events with XCORR > 16383 and YCORR > 1023.) Finally, each event weight was assigned to a pixel in the image based on their XCORR and YCORR values to build up the final image. The resulting 2D images are shown in Figure 3.

4. Data Analysis

The analysis consists of two independent parts, which are to characterize *(i)* the width of the 2D spectra in the cross-dispersion direction and *(ii)* the spectral resolution, both as functions of the focus position.

The thermal breathing of the telescope causes the actual focus position at any given time to differ from that commanded. Based on temperatures measured by on-board sensors, there are breathing models that may be used to determine the corrections. The results of the models are accessible via the HST focus model tool[1], which computes the focus offset with respect to the nominal value at a series of times. The WFC3/UVIS1 model, which is assumed to apply to COS, for the times covering the cenwave 800 focus sweep observations is shown in Figure 4. Also shown on the plot are the midpoints of the observations (red crosses) and their extents (red lines) at the interpolated focus values.
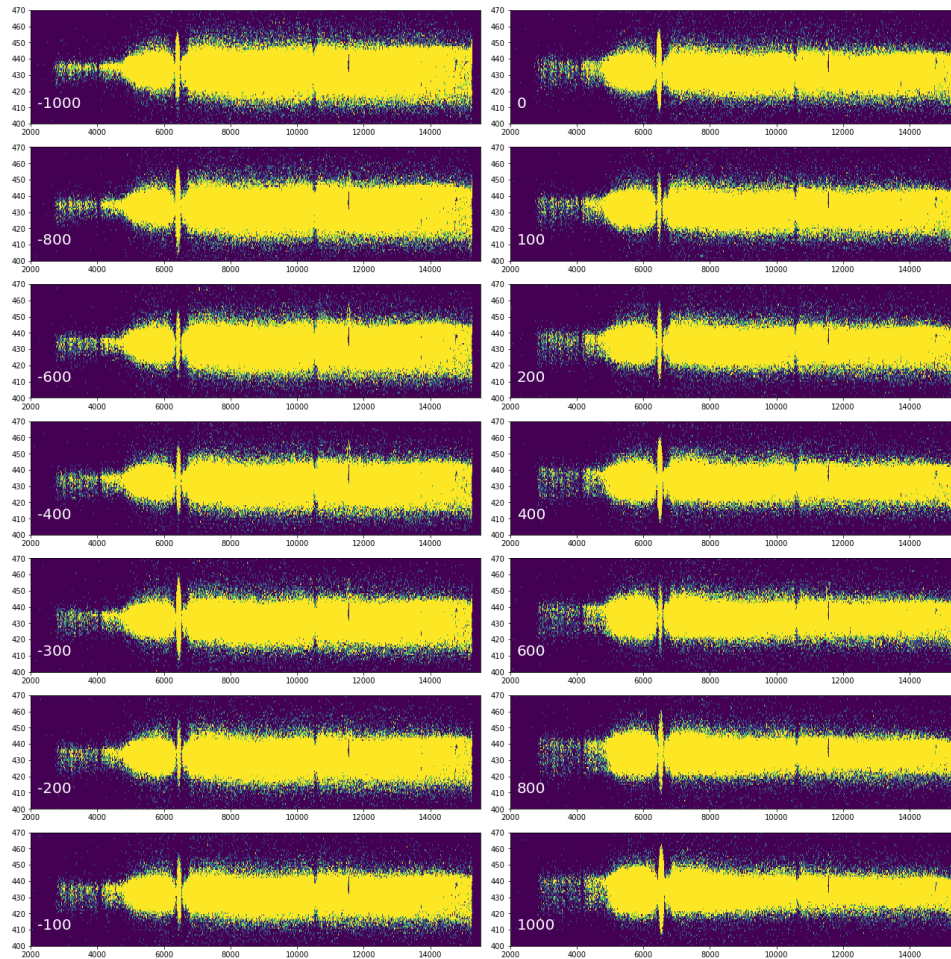
---

[1]http://focustool.stsci.edu/cgi-bin/control.py

Figure 3. 2D spectral images of AV 75, showing the detector region XCORR = [2000, 15500] and YCORR = [400, 470]. The labels are the commanded focus positions corresponding to each image.

Note that there are no model points between $\approx$ 0.58 and 0.63 (fractional time of day) and therefore for exposures 1 and 2, we used the model values closest to the observation times.

The focus offset in microns is multiplied by a conversion factor of 19.2 to give the correction in units of OSM1 steps, and the correction is ***subtracted*** from the commanded focus position to give the breathing-corrected value (Oliveira et al. 2013). The last column in Table 1 has the focus offsets that we use in our analysis. We note that measured values of the focus are available for $\approx$1 hour periods obtained a few times every year. The UVIS1 measurements were about 2.6 μm (50 steps) higher than the models on 2018 February 24 and up to 4 μm (77 steps) higher on 2018 April 29. However, our ultimate choice of the cenwave 800 focus was not sensitive to these levels of uncertainty in the actual focus positions.
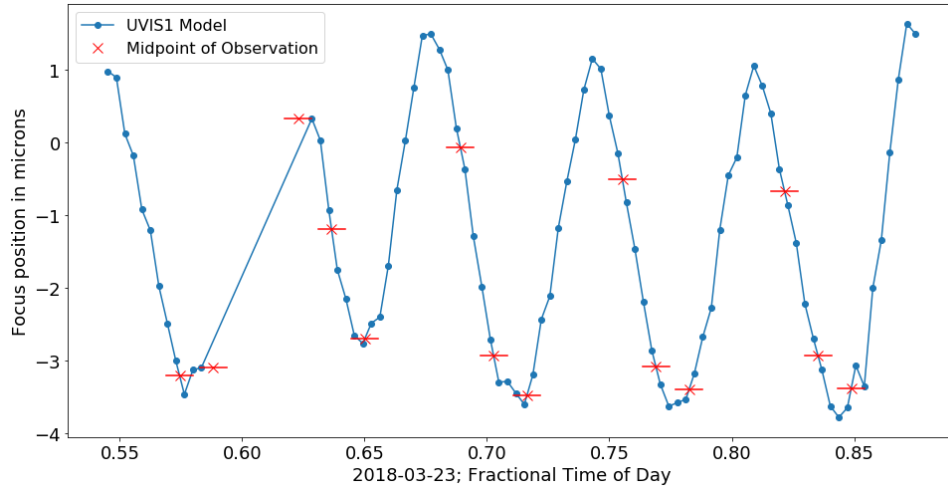
Figure 4. Breathing model used to obtain corrected focus values.

4.1 Cross-Dispersion Profile

The cross-dispersion profiles of the 2D spectra were extracted in six windows along the dispersion axis. The locations were chosen so that the entire short-wavelength region and representative portions of the rest of the spectral range were sampled. The cross-dispersion width varies sufficiently slowly in the short-wavelength region that three independent windows are adequate to characterize this variation as a function of focus position. This determined the 601 pixel width for each window. Figure 5 shows the extraction windows overlaid on the AV 75 spectrum obtained at focus offset = 0.0. The XCORR pixel ranges and their equivalent wavelengths are given in Table 2. The wavelength scale uses the dispersion solution (retaining the parabolic component and neglecting the sinusoidal term) for cenwave 800 at LP1 derived by Redwine et al. (2016):

$$\lambda\,(\text{Å}) = 701.65 + 0.07912 * XCORR + 3.9229^{-8} * XCORR^2.$$

The wavelength zero-point shifts by about $10\,\text{Å}$ between the two extreme focus positions. The windows for the cross-dispersion analysis are fixed in detector coordinates, so these wavelengths are approximate and given only as a guide.

For each image, the cross-cut profiles were first obtained by summing the spectrum over the 601 pixels of each window. Then, for each cross-cut, the background was calculated by averaging the profile counts between YCORR 630 and 710, which is a region well removed from the source spectrum and from the region where the lamp spectrum falls. The background was subtracted from the profile, and then the cumulative sum was calculated starting at the bottom of the box and ending at the top (YCORR = 343 to 523). The locations where the cumulative sums reached 0.5%, 2.5%, 97.5%, and 99.5% of their maximum values were identified. The outer and inner pairs bound the 99% and 95% enclosed energy widths, respectively.

Table 2.   Cross-Dispersion Profile Locations

Window #	Pixel Range (XCORR)	Wavelength Range (Å)
1	2900 – 3500	931.4 – 979.1
2	3500 – 4100	979.1 – 1026.7
3	4100 – 4700	1026.7 – 1074.4
4	5400 – 6000	1130.0 – 1177.8
5	7000 – 7600	1257.4 – 1305.2
6	10800 – 11400	1560.7 – 1608.7
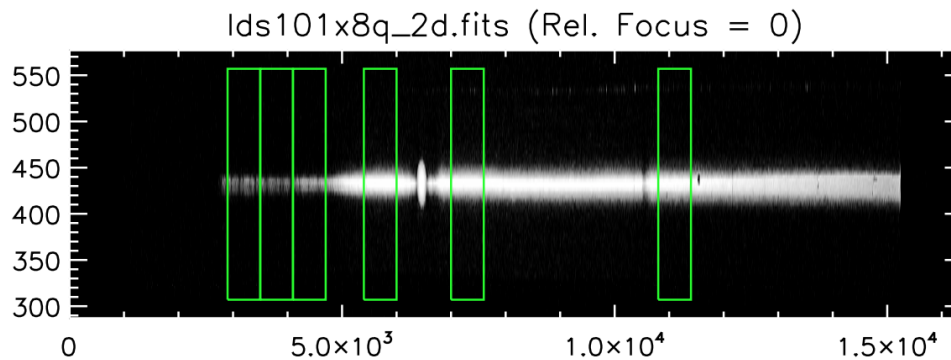
Figure 5. The 2D spectral image obtained at focus offset 0.0 with boxes overlaid to show where cross-dispersion widths were obtained.

The 95% and 99% enclosed energy widths were obtained for each of the windows for all focus position images. It was found that for all focus positions, the 99% limits were at YCORR locations where the counts were at the noise level. Therefore we used the 95% enclosed energy width as being more robustly representative of the astigmatic height, especially at the short wavelengths. Figure 6 is an example of the 95% limits determined for each of the windows in the focus offset = 0.0 2D spectrum.

The resulting 95% enclosed energy widths determined for the focus sweep data are shown in Figure 7. These widths are plotted for each of the six windows against the breathing-corrected focus. At all three short wavelength windows (1, 2, and 3), the equivalent width is minimum at the most negative focus offset and rises almost linearly with focus position. The longest wavelength window shows exactly the opposite trend, with the enclosed energy width decreasing linearly. The range of widths in the mid-range wavelengths, windows 4 and 5, are smaller; window 4 has a minimum near focus offset -650, and window 5 near $+150$.
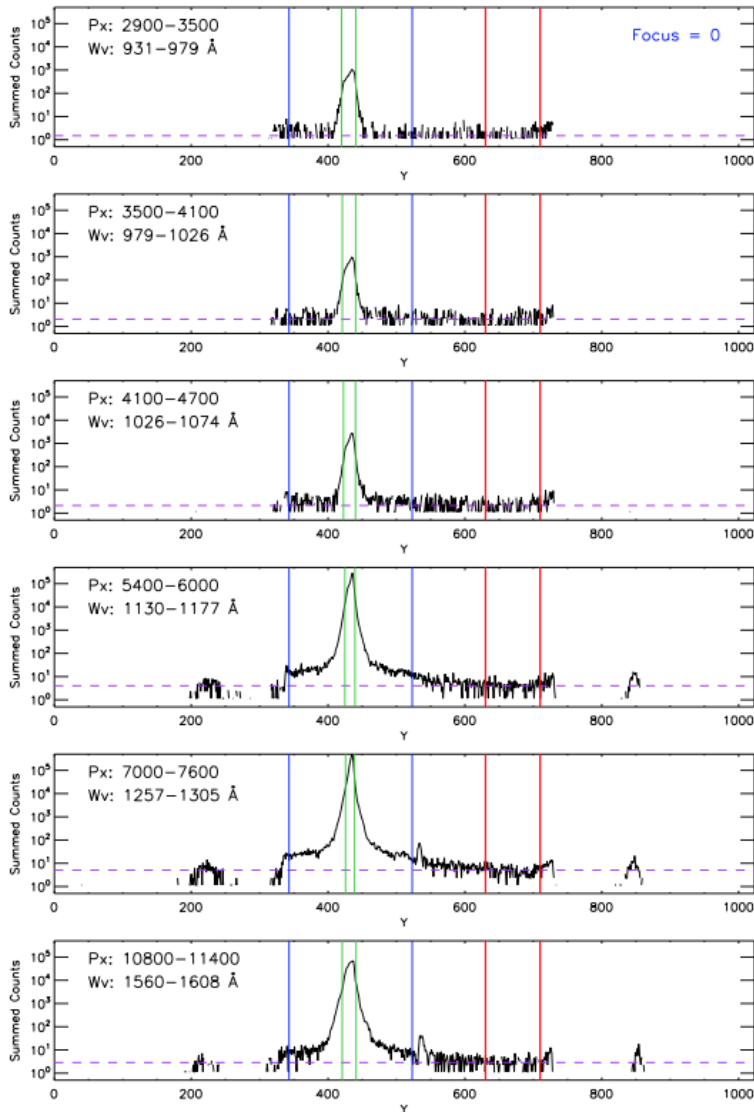
Figure 6. The profiles in the cross-dispersion direction across the focus offset = 0.0 spectrum at several locations in the dispersion direction, with the 95% enclosed energy widths shown as green vertical lines. The blue lines show the region over which the cumulative sum is taken, and red lines show the background region. Note that the summed counts (y-axis) are shown on a logarithmic scale.

4.2 Spectral Resolution

The spectral resolution is best obtained by measuring the observed widths of strong, narrow (unresolved) absorption or emission lines that span the wavelength range of a given observing mode. The focus position yielding the best spectral resolution (at some given wavelength) will then be the one for which the line is narrowest. However, for cenwave 800, due to the sensitivity cliff at 1150 Å, sources bright enough for this
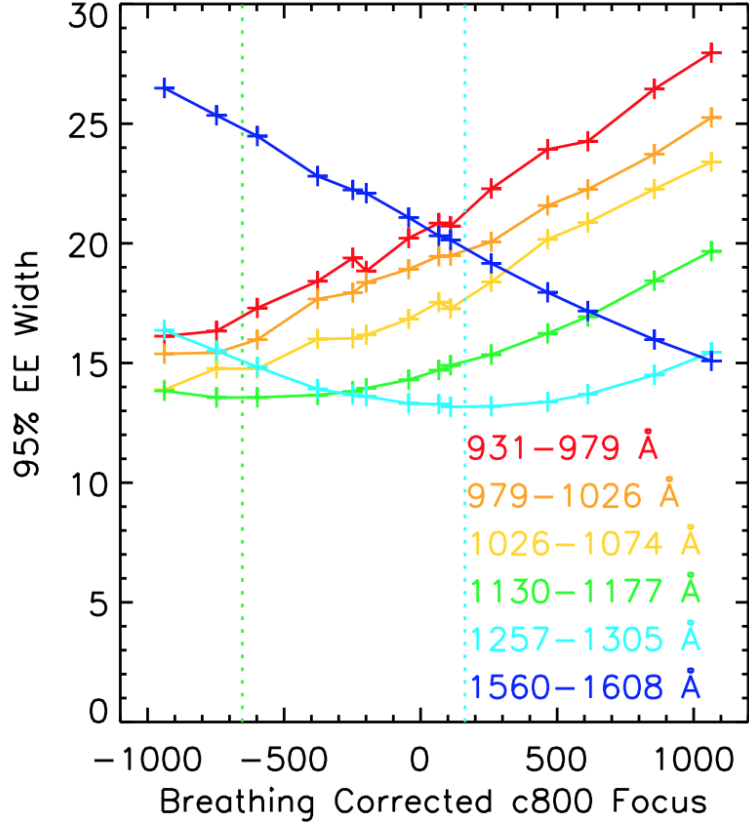
Figure 7. The 95% enclosed widths (in pixels) plotted as a function of the breathing-corrected focus for each of the chosen regions in the dispersion direction. The vertical dotted lines show where minima are reached for curves of the matching colors.

purpose at short wavelengths would violate the bright target limit at longer wavelengths. Therefore we use the autocorrelation function (ACF) method, introduced by Lennon et al. (2010) for the SMOV COS focus determination and used in subsequent focus analyses. The most recent of these for G140L modes (Oliveira et al. 2013; Fox et al. 2015, 2017) use AV 75 as the target.

The ACF is defined as the correlation of a spectrum with itself, offset by a fixed number of pixels, as a function of that offset. By definition it peaks at zero offset and is symmetric. In general, the width of the ACF increases with the width of absorption lines in the spectrum. (For the ideal case of a single line with a gaussian profile, the ACF is also a gaussian having a width that is $\sqrt{2}$ times the line width.) Thus, the focus position yielding the best resolution is the one for which the ACF width is the minimum.

We supplement the ACF analysis by measuring the width of the relatively strong Si II $\lambda1260$ line at each focus position. The STIS spectrum of AV 75 (presented in the accompanying ISR on the cenwave 800 wavelength calibration by Fischer et al. 2019) shows that the line may be marginally resolved at the best expected spectral resolution

Table 3. Cross-Dispersion Profile Locations

ACF Region #	Pixel Range (XCORR)	Wavelength Range (Å)	Focus Position Fits (quadratic, cubic)	Notes
1	2750 – 3450	919.5 – 971.1	18, −19	very shallow curve
2	5420 – 5800	1131.6 – 1161.9	−175, −211	points at +800, +1000 omitted in fit
3	8250 – 9000	1357.1 – 1416.9	−74, −134	well-behaved, the best case

for G140L/800. However, it is sufficiently narrow that the measured width may be used as a diagnostic for the trend in spectral resolution with focus position.

One-dimensional (1D) spectra were extracted from the 2D images by summing over 78 pixels in the cross-dispersion direction, YCORR = [403, 481]. Several broad regions of the spectrum, which avoided strong absorption lines but included weak lines, were selected for the analysis. The shifts in the wavelength scale zero-points for different focus positions were corrected by aligning the minima of absorption lines near the analysis window. The shift was defined to be 0.0 for the most negative focus position (−1000 commanded), which resulted in shifts ranging from 125 pixels at the short-wavelength end to 108 pixels at the long-wavelength end for the most positive position (+1000 commanded). For each region of the spectrum selected, the ACF was determined for offsets from 0 to 100 pixels. The scaling was defined so that the peak value was equal to 1.0 (at offset = 0 pixels). It was necessary to iterate on the exact region boundaries to exclude detector artifacts, make sure the correlation was not being done on noise, and to obtain reasonably well behaved ACFs. However, we were not able to find a region longward of $\sim$1420 Å suitable for ACF analysis.

Our final ACF analysis was done on three spectral regions, using the summed counts spectra. We used the offset (in pixels) at half-maximum of the ACF, which is a simple measurement independent of its functional form (and of the underlying spectral line shapes), to define its width. In most cases the ACFs were not gaussian or had non-gaussian wings, and profile fitting to obtain the width was not a viable option. For each spectral region, the ACF widths against the corrected focus offsets were fit using both quadratic and cubic functions. The regions selected for analysis and the fit results are given in Table 3. The wavelengths reported are based on the Redwine et al. (2016) dispersion solution (see Section 4.1) applied to the 0.0 shift pixels (i.e., the −1000 commanded focus observation). The spectra, ACFs, and fits to the widths are shown in Figure 8.

The curve of ACF widths is very shallow for the short-wavelength region and does not strongly discriminate among the focus positions. The other two regions show clear minima, which lie in the range −211 to −74 offset steps. Equally importantly, the ACF widths become larger at focus offsets less than −500. This is true for all three spectral windows analyzed, and it is most pronounced for region 3.
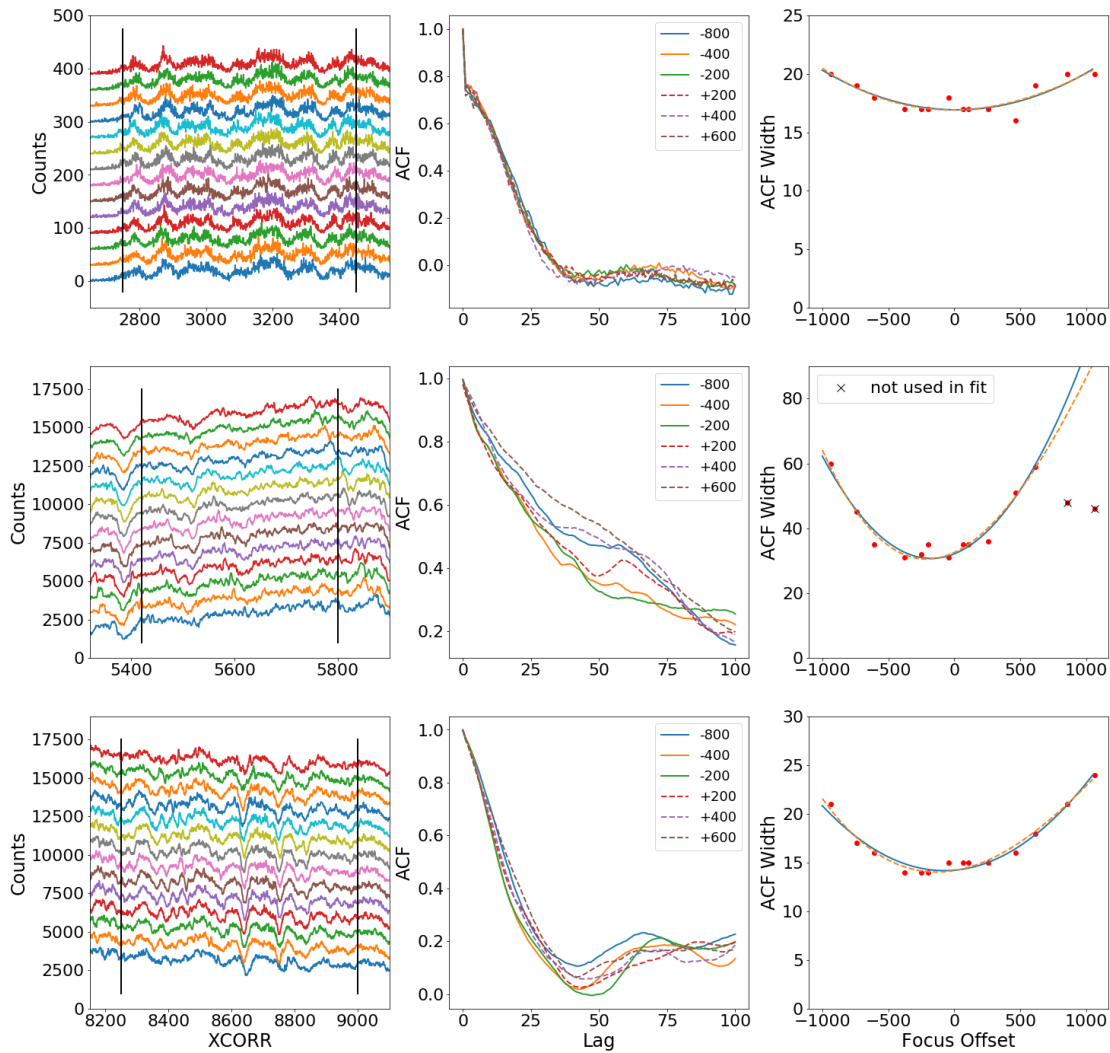
Figure 8. The counts spectra (left), ACFs (middle), and the ACF widths overlaid with quadratic and cubic fits (right) are shown for three regions of the spectrum (Table 3). The counts spectra have been aligned in wavelength space and offset for clarity. The solid vertical lines show the regions used for obtaining the ACFs. Note the extremely low counts in the short-wavelength region (top row).

To check the trend of line width with focus position we selected the relatively strong, isolated Si II line at 1260 Å. The line was fit using a single gaussian with a constant continuum and negative amplitude. Although we do not expect the line shape to be a gaussian, this simple fit is sufficiently robust, and it is adequate for our purposes. The ACF analysis was done for a 150 pixel region around the line in order to check for consistency. Figure 9 (left panel) shows the counts spectra in the window. (A visual inspection shows that the line broadens significantly towards the extreme focus positions.) The right panel shows the gaussian fit widths and the ACF widths plotted
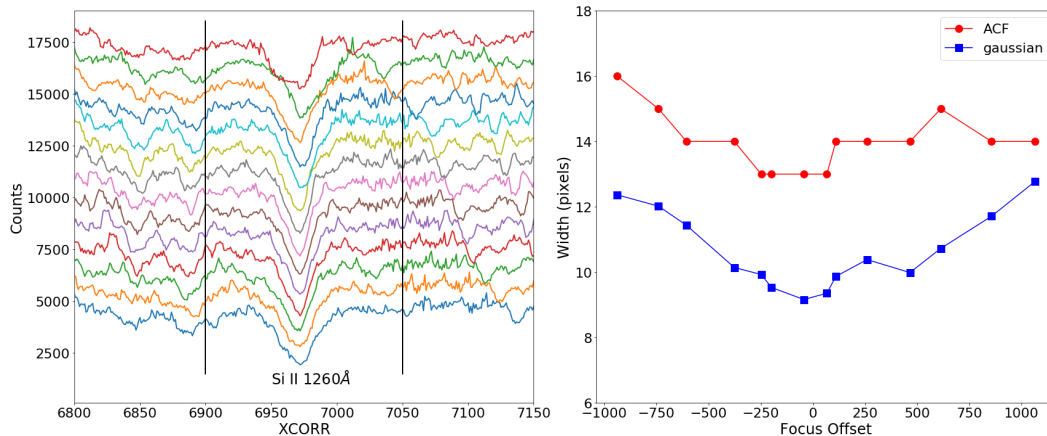
Figure 9. Left panel: counts spectra of the region around the Si II line at 1260 Å, plotted against XCORR pixel number. Spectra obtained at different focus positions are offset in the y-direction. Right panel: the gaussian widths of the line and the widths of the ACFs are plotted against the focus offset.

against the corrected focus positions. The key result is that the spectral resolution is significantly degraded at focus offsets below -500 compared with offsets around 0.

5. Selecting the Focus

The primary criterion for the optimal focus position for the new cenwave 800 mode is to minimize the astigmatic height of a point source spectrum in the 915–1100 Å wavelength region. A secondary criterion, quantitatively less well defined, was to keep the spectral resolution as close as possible to the maximum achievable for the mode. We have found from the focus sweep data that the astigmatic height at short wavelengths is the smallest for the most negative focus offset and increases approximately linearly with the offset steps. A precise value for the focus position yielding the best spectral resolution could not be measured. Rather, we found that the resolution is close to the maximum achievable over a range of focus offsets from about -200 to 0, and a clear degradation of at least 10%, based on the measured line widths, occurs below -400 and above $+200$. We note that the longer wavelength region does not factor into the choice of focus. Figure 10 provides a graphical summary of our results.

Based on these results, a focus offset value of -400 was chosen for cenwave 800. The 95% enclosed energy width is about 2 pixels larger than the minimum value in the XCORR = 2900 to 3500 pixel range, and there is little or no degradation of the spectral resolution. The absolute focus position for G140/800 is selected to be $-400 - 1087 = -1487$ absolute steps. The selected focus value was used in subsequent calibration programs that are described in accompanying COS ISRs, and it is currently in use for regular cenwave 800 observations.
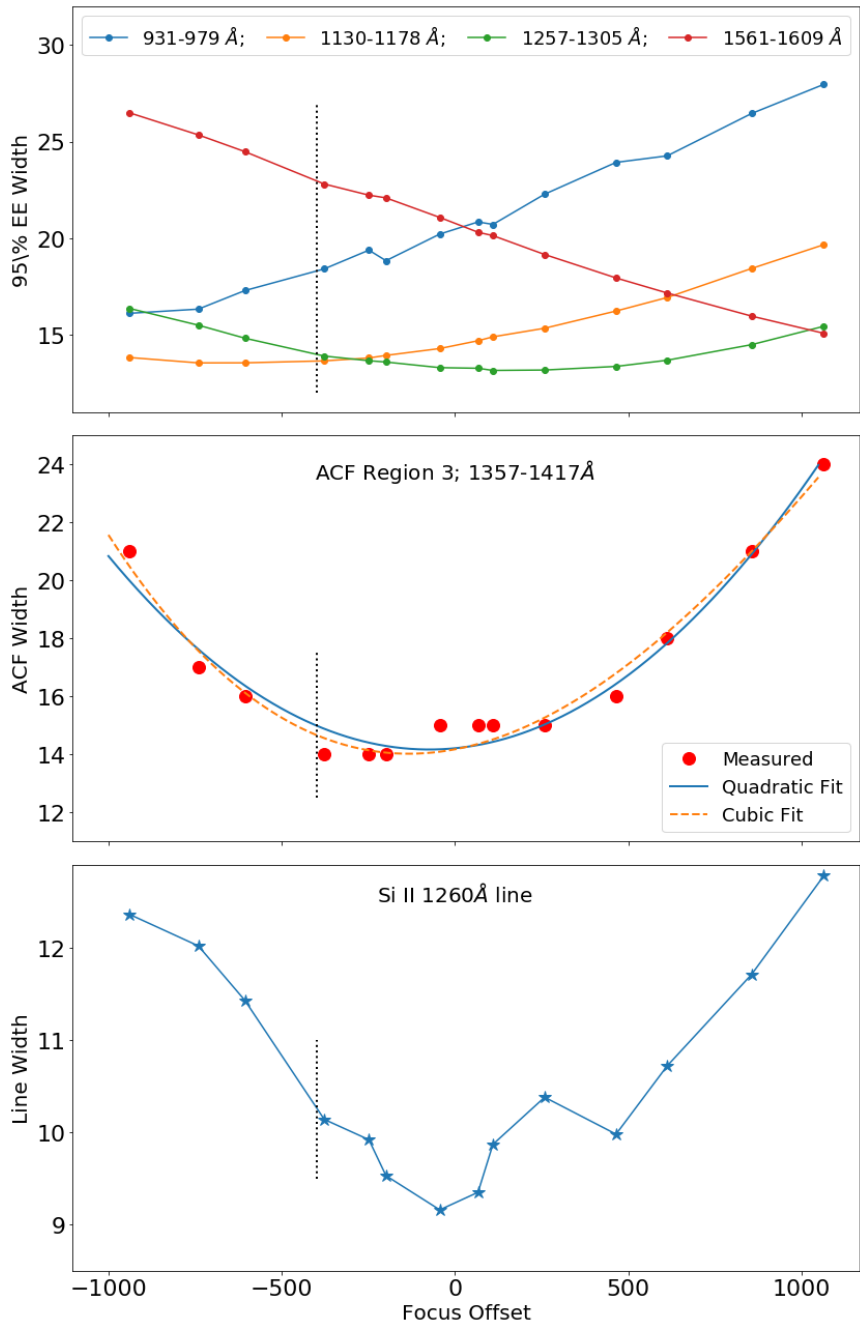
Figure 10. Plots summarizing the results of our analyses. The cross-dispersion widths, in YCORR pixels, for four of the six windows (top), the widths (XCORR pixel offsets) of the ACFs and the fits for region 3 (middle), and the Si II line width in XCORR pixels (bottom) are plotted against the focus offsets. The optimal focus chosen, OFFSET = −400, is shown by the vertical line on each of the plots.

The scripts used for the data calibration, image creation, and the analyses have been placed in the `cos/newcenwave_c800` repository on the internal STScI GitLab site.

Acknowledgments

Change History for COS ISR 2019-01

Version 1: 8 July 2019 – Original Document

References

De Rosa, G., et al. 2018, COS ISR 2018-09, "Cycle 24 COS/FUV Spectroscopic Sensitivity Monitor"

Fischer, W. J., Magness, C. R., Sankrit, R., & Oliveira, C. 2019, COS ISR 2019-05, "The Dispersion Solution for the New COS/FUV Cenwave G140L/800"

Fox, A., Oliveira, C., Penton, S., et al. 2015, COS ISR 2015-01, "The COS/FUV Focus Sweep Program at Lifetime Position 3 (LENA2/13635)"

Fox, A., Penton, S., & Taylor, J. 2017, COS ISR 2017-17, "Focusing the COS/FUV G160M and G140L Gratings at Lifetime Position 4"

Ghavamian, P. 2012, COS ISR 2012-01, "COS FUV Focus Determination for the G140L Grating"

Lennon, D., Oliveira, C., Hartig, G., et al. 2010, COS ISR 2010-07, "SMOV: COS FUV Focus Determination"

Oliveira, C., Bostroem, A., & Osterman, S. 2013, COS ISR 2013-01, "Second COS FUV Lifetime Position Results from the Focus Sweep Enabling Program, FENA3 (12796)"

Redwine, K., McCandliss, S. R., Zheng, W., et al. 2016, PASP, 128, 105006

Appendix A

The primary motivation for introducing the cenwave 800 mode is to allow a much reduced background at wavelengths between 912 and 1100 Å compared to the existing cenwave 1280 mode. The difference between the two modes is illustrated in Figure 11.
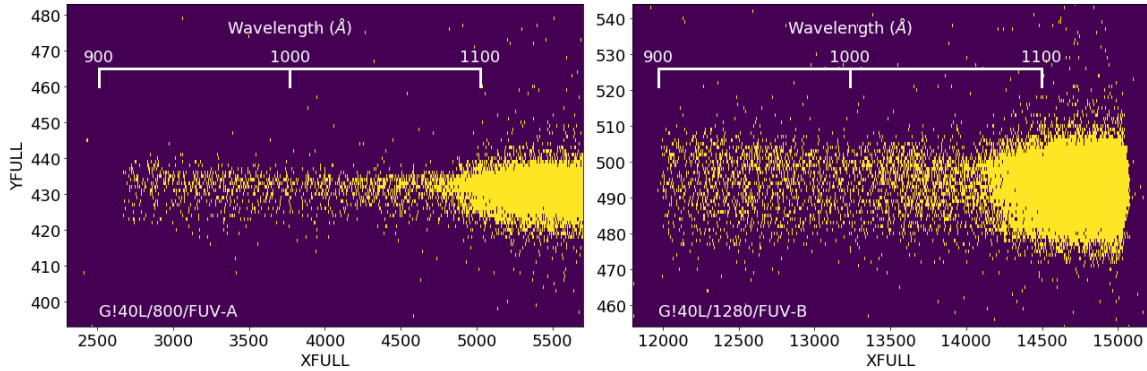

Figure 11. COS 2D spectra of the flux standard WD 0308−565, obtained using G140L/800/FUVA (left) and G140L/1280/FUVB (right). The data were obtained in the cenwave 800 and LP4 flux calibration programs, PIDs 15483 and 14910, respectively. The exposure times were 363 s for the cenwave 800 observation and 667 s for the cenwave 1280 observation. The spectra are shown in detector coordinates, and they are displayed so the profile centers along the cross-dispersion (YFULL) axis are aligned. The smaller astigmatic height for cenwave 800 is visually apparent. To confirm that this was not an effect of the different exposure times, we obtained the normalized cross-dispersion profiles of the spectra summed between 920 and 1070 Å and measured the full-width at half-maximum (FWHM) for each case. The FWHM of the cenwave 800 cross-dispersion profile was about half that of the cenwave 1280 profile.